

# Spin blockade in electron transport through single $Mn_{12}$ molecular magnets

H. B. Heersche,\* Z. de Groot, J. A. Folk,<sup>†</sup> and H. S. J. van der Zant

*Kavli Institute of Nanoscience, Delft University of Technology, Lorentzweg 1, 2628 CJ Delft, The Netherlands*

C. Romeike and M. R. Wegewijs

*Institut für Theoretische Physik A, RWTH Aachen, 52056 Aachen, Germany*

L. Zobbi<sup>1</sup>, D. Barreca<sup>2</sup>, E. Tondello<sup>2</sup>, and A. Cornia<sup>1</sup>

<sup>1</sup>*Department of Chemistry, University of Modena and Reggio Emilia and INSTM, via G. Campi 183, I-41100 Modena, Italy and*

<sup>2</sup>*ISTM-CNR, Department of Chemistry, University of Padova and INSTM, Via Marzolo 1, I-35131 Padova, Italy*

(Dated: December 21, 2018)

We report transport measurements through a single-molecule magnet, the  $Mn_{12}$  derivative  $[Mn_{12}O_{12}(O_2C-C_6H_4-SAc)_{16}(H_2O)_4]$ , in a single-molecule transistor geometry. Thiol groups connect the molecule to gold electrodes that are fabricated by electromigration. Striking observations are regions of complete current suppression and excitations of negative differential conductance on the energy scale of the anisotropy barrier of the molecule. Transport calculations, taking into account the high-spin ground state and magnetic excitations of the molecule, reveal a blocking mechanism of the current involving non-degenerate spin multiplets.

PACS numbers: 85.65.+h ,73.23.Hk ,73.63.Kv 75.50.Xx

During the last few years it has been demonstrated that metallic contacts can be attached to individual molecules allowing electron-transport measurements to probe the intrinsic properties of the molecules. Coulomb blockade and the Kondo effect, typical signatures of a quantum dot, have been observed at low temperature in a single-molecule transistor geometry [1, 2, 3]. In the Coulomb blockade regime, vibrational modes of the molecule appear as distinct features in the current-voltage ( $I - V$ ) characteristics [4, 5, 6]. Conformational, optical or magnetic properties of molecules may also affect electron transport. With respect to the latter, an interesting class of molecules is formed by the single-molecule magnets (SMMs). These molecules show magnetic hysteresis due to their large spin and high anisotropy barrier, which hampers magnetization reversal. The prototypal SMM,  $Mn_{12}$ -acetate, has total spin  $S = 10$  and an anisotropy barrier of about 6 meV [7]. Spin excitations play an important role in the magnetization reversal process through quantum tunneling of the magnetization (QTM) [8]. Although the electronic and magnetic properties of SMMs have been studied intensively on bulk samples and thin films [9, 10, 11, 12, 13], the effect of the high-spin ground state on electron transport in isolated molecules remains an unexplored topic [14].

In this Letter we discuss transport through individual SMMs that are weakly coupled to gold electrodes (see Fig. 1). Experimental data show low-energy excited states with a strong negative differential conduc-

tance (NDC) and regions of complete current suppression (CCS). For comparison, we have modelled tunneling through a single  $Mn_{12}$  molecule taking into account its unique magnetic properties. The magnetic anisotropy in the molecule gives rise to an easy axis, which we define as the  $z$ -axis. Our calculations include selection rules for the molecular spin  $S$  and its  $z$ -axis projection  $M$ , as well as QTM perturbations. Sequential tunnel processes result in spin-blockade of the current, explaining the observed NDC and CCS. This effect is different from conventional spin blockade [15] where effects of  $M$  selection rules are not observable due to spin-degeneracy.

We use the single-molecule magnets  $[Mn_{12}O_{12}(O_2C-R-SAc)_{16}(H_2O)_4]$  ( $Mn_{12}$  in the rest of the text), where  $R=\{C_6H_4, C_{15}H_{30}\}$ . Both are tailor-made  $Mn_{12}$ -acetate

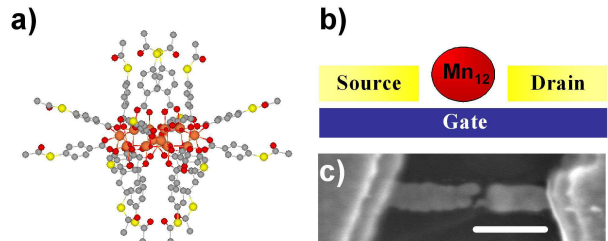


FIG. 1: (a) Side view of a  $Mn_{12}$  molecule with tailor made ligands containing acetyl-protected thiol end groups ( $R=C_6H_4$ ). Atoms are color labelled: Manganese (orange), oxygen (dark red), carbon (gray), sulfur (yellow). The diameter of the molecule is about 3 nm. (b) Schematic drawing of the  $Mn_{12}$  molecule (red circle) trapped between electrodes. A gate can be used to change the electrostatic potential on the molecule enabling energy spectroscopy. (c) Scanning electron microscopy image of the electrodes. The gap is not resolvable. Scale-bar corresponds to 200 nm.

\*Electronic address: hubert@qt.tn.tudelft.nl

<sup>†</sup>Present Address: Department of Physics, University of British Columbia, Vancouver, Canada

derivatives [16]. These molecules feature thiol groups in the outer ligand shell and consequently exhibit a strong affinity for gold surfaces [12, 17]. Beside ensuring robust tethering of the clusters to the surface, the ligands are also believed to serve as tunnel barriers, so that the molecule is only weakly coupled electronically to the gold. Its electronic and magnetic properties are therefore preserved. The diameter of the molecule (core plus ligands) is about 3 nm for  $R=C_6H_4$  and 5 nm for  $R=C_{15}H_{30}$ . In this paper we focus on the spin related transport features that are measured on the  $R=C_6H_4$  derivative, which is depicted in Fig. 1(a). The  $R=C_{15}H_{30}$  derivative was used to verify that the electronic transport properties are related to the core of the molecule and not to the ligands.

Electromigration [18] produced the nanometer-scale gaps in which the molecules were trapped. We fabricated thin ( $\sim 10$  nm) gold wires (width 100 nm, length 500 nm) on top of Al/Al<sub>2</sub>O<sub>3</sub> gate electrodes using e-beam lithography. The wires were contacted by thick (100 nm) gold leads. The samples were cleaned in acetone and isopropanol, descummed with an oxygen plasma, then soaked in a 0.1 mM Mn<sub>12</sub>-solution containing a catalytic amount of aqueous ammonia (to promote deprotection of the -SAC groups, see Ref. [17]) for at least 1 hour. After taking a sample out of the solution it was dried in a nitrogen flux and mounted in a He4 system with a 1 K pot. The bridges were electromigrated in vacuum at room temperature by ramping a voltage across the wire while monitoring the current using a series resistor of 10  $\Omega$ . The junctions broke at about 1 V.

After breaking, the samples were cooled down to 4 K and the junction conductances were measured. Although about 10 % of 200 junctions showed Coulomb blockade related features, only four samples were stable enough for detailed measurements [19]. In Fig. 2(a) we plot the differential conductance  $G$  as a function of gate voltage ( $V_g$ ) and bias voltage ( $V_b$ ) for one such a device ( $T = 3$  K,  $R=C_6H_4$ ). The lines separating the conducting regions from the diamond-shaped Coulomb blockade regions have different slopes for the three different charge degeneracy points. If we assume that the capacitive coupling of the molecule is independent of the charge state, this observation indicates that the degeneracy points belong to different molecules. The current within a given transport region is, however, determined by an individual molecule. Lines in each transport region correspond to the onset of transport through excited states of the molecule. The low-energy features of the different transport regions, are not identical. This may be due to the fact that they belong to different charge transitions (see calculations below).

We have observed an excitation at  $14 \pm 1$  meV in all 6 of the stable transport regions that were observed in the four samples. This excitation is indicated with arrows in Fig. 2(c-f) and Fig. 3(a). Although the physical origin of this excitation remains unclear, it appears to be a fingerprint of the molecule. Such a fingerprint is

needed since small metal grains that are formed during electromigration can mimic the transport properties of single-molecules [20, 21, 22]. Moreover, we have studied the electromigration process extensively and found that the gap size can be tuned by the total (on- and off-chip) series resistance [23]. A relatively large series resistance (200  $\Omega$ ) has been used to create a gap larger than  $\sim 1$  nm. Using this technique, we did not measure any conductance up to 1 V in 50 control samples without molecules deposited.

The focus of this paper is on transport features at low-energy ( $\lesssim 5$  meV): a region of complete current suppression (CCS) and a strong negative differential conductance (NDC) excitation line in the stability diagrams. Both

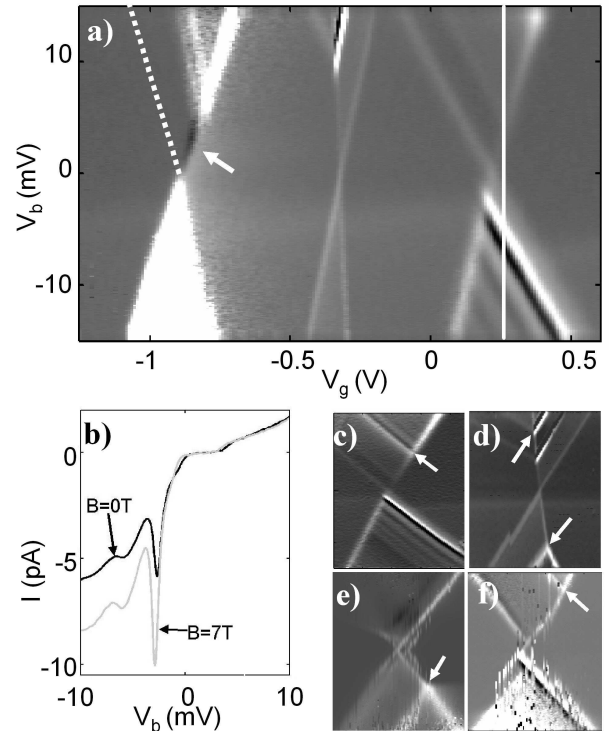


FIG. 2: (a) Differential conductance (gray-scale) as a function of gate voltage ( $V_g$ ) and bias voltage ( $V_b$ ) ( $T = 3$  K,  $R=C_6H_4$ ). A region of complete current suppression (left degeneracy point, arrow) and low-energy excitations with negative differential conductance (right degeneracy point) are observed. The dashed line near the left degeneracy point indicates the suppressed diamond edge. (gray-scale from -0.8 nS [black] to 1.4 nS [white]). (b)  $I - V_b$  at the gate voltage indicated in (a) with a line. NDC is clearly visible as a decrease in  $|I|$  upon increasing  $|V_b|$ . Upon applying a magnetic field, current is increased for negative bias. (c-f) Same as (a) for 4 transport regions in which the 14 meV excitation is indicated with arrows. Bias voltage ranges are:  $V_b = \pm 30$  mV,  $V_b = \pm 20$  mV,  $V_b = \pm 25$  mV,  $V_b = \pm 15$  mV, respectively. (c,d) are the right and center charge transport regions of the sample in (a), respectively. (e,f) are measured in devices with the  $R=C_{15}H_{30}$  ligands.

are visible in Fig. 2(a). At the left degeneracy point in this figure the current is fully suppressed at positive bias voltage above the left diamond edge (dashed line). Transport is restored beyond an excitation that lies at 5 meV. Remarkably, the right diamond edge *does* continue all the way down to zero bias, defining a narrow strip ( $\sim 1$  mV) where transport is possible. In the right conductive regime in Fig. 2(a), two excitations at an energy of 2 meV and 3 meV are the most pronounced features. The 2 meV excitation is visible as a bright line with positive differential conductance (PDC); the 3 meV excitation as a black line (NDC). NDC is also clearly visible in the  $I - V_b$  plot in Fig. 2(b). In Fig. 3, the PDC and NDC excitations at 2 meV and 3 meV are shown for another device. For negative bias, the 14 meV excitation is also observed. We emphasize that we never observed the low-energy features in bare gold samples or in samples with other molecules deposited despite measuring over one thousand junctions in total.

The observed NDC and CCS follow theoretically from calculations that combines the standard sequential tunneling theory with the spin-Hamiltonian description of the high-spin ground state and its ladder of spin excited states (see Fig. 4). Both the total spin of the molecule  $S$  and its projection  $M$  on the intrinsic anisotropy axis of the molecule ( $z$ -axis) are important. Qualitatively, NDC and CCS can be understood as follows: The spin-selection rules  $|\Delta S|, |\Delta M| = \frac{1}{2}$  apply to adding or subtracting an electron. Spin states of the molecule which differ by more than  $\frac{1}{2}$  from the ground states are accessible via subsequent tunnel processes, but only if each step in the sequence is energetically allowed. A sequence of tunnel processes can result in a non-equilibrium population of certain excited states that can only be depopulated slowly by a violation of the spin-selection rules induced by QTM. Transport is then hindered or blocked at sufficiently low temperatures leading to NDC or CCS.

Our calculations (see Fig. 4) take as a starting point the basic spin-Hamiltonian for a SMM in charge state  $N$  ( $N = n$  neutral,  $N = n - 1$  oxidized,  $N = n + 1$  reduced) and two electronic states  $\alpha = 0, 1$  for each charge state (energy splitting  $\Delta_N$ ) and total spin  $S_{N\alpha}$ :

$$H_{N\alpha} = -D_{N\alpha}S_z^2 + B_2(S_x^2 - S_y^2), \quad (1)$$

where  $D_{N\alpha} > 0$  is an anisotropy constant and  $B_2$  the lowest order QTM perturbation due to deviations from perfect axial symmetry. For  $B_2 = 0$  this Hamiltonian gives rise to a ladder consisting of the  $2S_{N\alpha} + 1$  different  $M$  states, see Fig. 4(a). The states  $M = \pm S_{N0}$  are degenerate ground states of the molecule and are separated by the magnetic anisotropy barrier (MAB). Transition rates between spin states upon adding or subtracting an electron are determined by Clebsch-Gordan coefficients and spin selection rules. We consider weak QTM (small  $B_2$ ) where this picture is still correct up to weak violations of the spin-selection rules which are taken into account. Electronic- and spin-excitation relaxation rates are assumed to be much smaller than the tunnel rates [24].

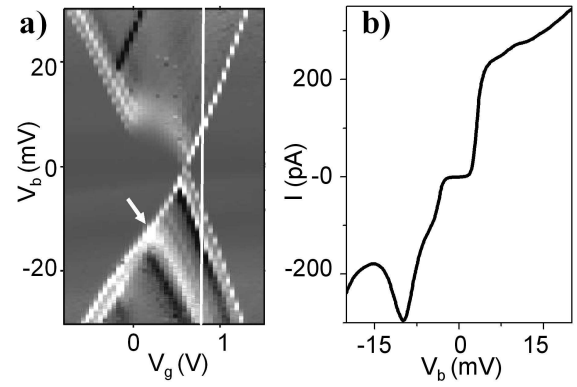


FIG. 3: (a) Differential conductance (grayscale) as a function of gate voltage ( $V_g$ ) and bias voltage ( $V_b$ ) for another device ( $T = 1.5$  K,  $R = C_6H_4$ ) in which the 2 meV and 3 meV excitations are also observed (negative bias). The 14 meV excitation is indicated by a white arrow. The origin of the step in the diamond edge at positive bias is unclear, but most likely not related to the magnetic properties of the molecule. (gray-scale from -3 nS [black] to 10 nS [white]) (b)  $I - V_b$  along the line in (a).

Measurements show that the MAB of the neutral  $Mn_{12}$  molecule ( $D_{n0}S_{n0}^2$ ) equals 5.6 meV [16]. Recently, it has been demonstrated that the first excited spin state in a neutral  $Mn_{12}$  derivative has  $S_{n,1} = 9$  and lies about  $\Delta_n = 4$  meV above the  $S_{n,0} = 10$  ground state [25], as theoretically predicted by Park et al. [26]. However, little is known about positively- or negatively- charged  $Mn_{12}$  clusters [26], except that one-electron reduced species have a  $S_{n+1,0} = 9\frac{1}{2}$  ground state and a lower MAB [27]. Therefore our calculations require a choice of parameters. Because the conventional spin-blockade (of the zero-bias conductance) is not observed [15] we can restrict the spin state transitions by  $|\Delta S| = \frac{1}{2}$  relative to  $S = 10$ . Assuming that the MABs for charged molecules are roughly of the same order of magnitude as for the neutral molecule we have done an extensive sweep through the parameter space, varying  $D_{N,\alpha}$ ,  $\Delta_{N,\alpha}$ ,  $B_2$ , and the ratio of the coupling with the two leads,  $\Gamma_L/\Gamma_R$ . We found that NDC and CCS occur whenever (i) the MAB is charge state dependent (ii) the spin multiplets within a charge state overlap in energy ( $D_{N0}S_{N0}^2 > \Delta_N$ ).

A sequence of tunnel events resulting in CCS is indicated in Fig. 4(b) for the  $n - 1 \leftrightarrow n$  transition and parameters listed in Ref. [28]. At low bias, only the ground-state transition ( $\alpha = 0, M = 9\frac{1}{2}_{n-1} \leftrightarrow (0, 10)_n$ ) is in the bias window. Upon increasing the bias voltage, other transitions [like  $(0, 8\frac{1}{2})_{n-1} \leftrightarrow (0, 10)_n$ ] become energetically allowed, but they do not obey the spin selection rules. The first spin-allowed transition  $(1, 9\frac{1}{2})_{n-1} \leftrightarrow (0, 10)_n$  requires an extra energy  $\Delta_{n-1}$  relative to the ground state transition. When this transition is in the bias window, however, the blocking state  $(0, 8\frac{1}{2})_{n-1}$  is immediately populated via the  $(1, 9\frac{1}{2})_{n-1} \leftrightarrow (0, 9)_n$  and

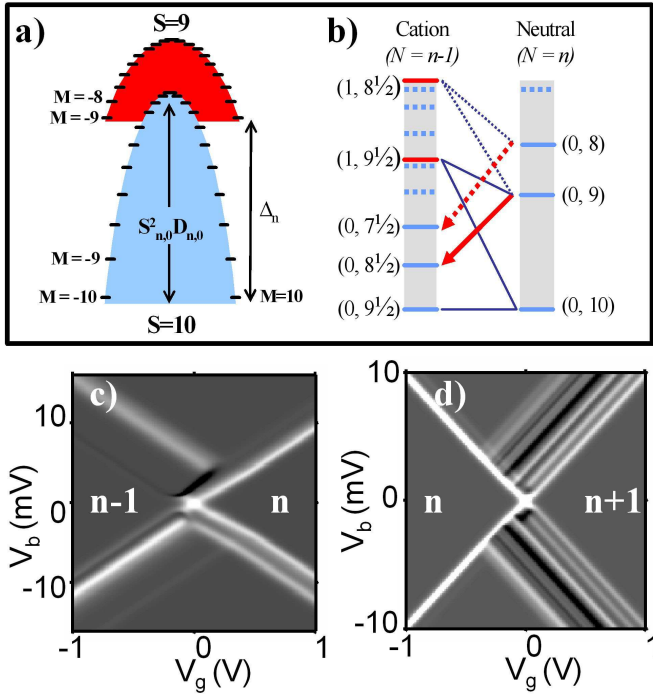


FIG. 4: Model calculations. (a) Energy diagram of the  $S_z$  states for the electronic ground state ( $\alpha = 0$ , blue) and first excited state ( $\alpha = 1$ , red) of the neutral molecule ( $N = n$ ). (b) Schematic drawing of the transitions involved in the complete current suppression process (CCS). For the cation, two spin manifolds, both with total spin  $S = 9\frac{1}{2}$  and with energy separation  $\Delta_{n-1} = 1.3$  meV are involved. The numbers in brackets denote  $(\alpha, M)$ . Dark blue lines are spin transitions induced by single-electron tunnel process. A sequence of tunnel processes can lead to the population of a blocking state (red arrow) which cannot be depopulated at low bias voltage due to spin selection rules. At higher bias other transitions (dashed) result in the occupation of a new blocking state. Note, that an equivalent diagram exists for the degenerate states with a negative  $M$  value. (c,d) Differential conductance (grayscale from -0.8 [black] to 1 [white] a.u.) modeling CCS (c) and NDC (d). Parameters are listed in Ref. [28]

$(0, 8\frac{1}{2}) \leftarrow (0, 9)_n$  (red arrow) transitions. Since spin selection rules prevent this state to depopulate via  $(0, 10)_n$ , transport is blocked. Contrary to expectation, an increase in bias does not lift the blockade because with increasing bias the role of the blocking state is passed

on to the next state (dashed arrow in Fig. 4(b)), until finally the  $M = \pm\frac{1}{2}$  state is liberated. Due to this “relay” of blocking states the suppression extends up to the energy scale of the MAB of the neutral molecule. The observed 5 meV is in good agreement with the value of susceptibility measurements mentioned above. In contrast with ordinary spin blockade, the current is not blocked in the narrow region where only the ground states of the molecule are accessible. This is also observed experimentally.

Excitations with NDC are obtained for the  $n \leftrightarrow n + 1$  transition (see Fig 4(c)). The mechanism is similar as for CCS, but a lower MAB of the charged ground state spin multiplet [28] leads to low-energy excitations that do not provide a path to a blocking state. As a result, PDC lines precede the NDC line at 3 meV, which belongs to the first available blocking state  $(0, 6\frac{1}{2})_{n+1}$ .

Other parameter choices than the ones listed in Ref. [28] give similar results so that we cannot unambiguously identify the spin and charge transitions in our measurements. We note that the blockade mechanism does not depend critically on QTM since the molecular magnet is driven into non-equilibrium states by electron tunneling. The increase of the current upon applying a magnetic field, Fig. 2(b), may be related to the mixing of spin eigenstates, allowing transitions which are inhibited due to spin selection rules in the absence of a field. Unfortunately, the angle of the external field with respect to the easy axis of the molecule is unknown, so that a more quantitative analysis is difficult.

In conclusion, we have measured transport through single  $\text{Mn}_{12}$  molecules that are weakly coupled to gold electrodes. Current suppression and negative differential conductance on the energy scale of the anisotropy barrier have been observed. Calculations reproduce these features, which are due to sequential tunnel processes, involving spin excitations of both charge states. These results provide a new direction in the study of single-molecule magnets and possibly lead to electronic control of nano-magnets.

HBH thanks H. Park’s research group (Harvard) for their help and CR and MRW thank H. Schoeller for discussions. This work was supported by FOM, NWO (HBH, ZdG, HSJvdZ), the EU-RTN program on spintronics (MRW), the HP Program RTN-QUEMOLNA, NOE”MAGMANET”, and Italian MIUR (LZ, AC).

---

[1] J. Park et al., *Nature* **417**, 722 (2002).  
[2] W. Liang et al., *Nature* **417**, 725 (2002).  
[3] S. Kubatkin et al., *Nature* **425**, 698 (2003).  
[4] H. Park et al., *Nature* **407**, 57 (2000).  
[5] L. H. Yu et al., *Phys. Rev. Lett.* **93**, 266802 (2004).  
[6] A. N. Pasupathy et al., *Nano Lett.* **5** (2005).  
[7] R. Sessoli et al., *Nature* **365**, 141 (1993).  
[8] D. Gatteschi and R. Sessoli, *Angew. Chemie Int. Ed.* **42**, 268 (2003).  
[9] J. R. Friedman et al., *Phys. Rev. Lett.* **76**, 3830 (1996).  
[10] E. J. L. McInnes et al., *J. Am. Chem. Soc.* **124**, 9219 (2002).  
[11] M. Cavallini et al., *Angew. Chem. Int. Ed.* **44**, 888 (2005).  
[12] M. Mannini et al., *Nano Lett.* **5**, 1435 (2005).  
[13] K. Kim et al., *Appl. Phys. Lett.* **85**, 3872 (2004).  
[14] G.-H. Kim and T.-S. Kim, *Phys. Rev. Lett.* **92**, 137203 (2004).  
[15] D. Weinmann, W. Häusler, and B. Kramer, *Phys. Rev.*

Lett. **74**, 984 (1995).

[16] Supplementary information on the synthesis and analysis of the Mn<sub>12</sub> (R=C<sub>6</sub>H<sub>4</sub>) samples on request.

[17] A. Cornia et al., Angew. Chem. Int. Ed. **42**, 1645 (2003).

[18] H. Park et al., Appl. Phys. Lett. **75** (1999).

[19] The yield was similar for both types of derivatives. Two of the stable samples were obtained with the R=C<sub>15</sub>H<sub>30</sub> derivative.

[20] R. Sordan et al., Appl. Phys. Lett. **87**, 013106 (2005).

[21] A. A. Houck et al., Nano Lett. **5**, 1685 (2005).

[22] H. B. Heersche et al., Condmat/0509100 (2005).

[23] H. van der Zant et al., Faraday discussions **DOI: 10.1039/b506240n** (2006).

[24] W. Wernsdorfer et al., Eur. Phys. Lett. **50**, 552 (2000).

[25] K. Petukhov et al., Phys. Rev. B **70**, 054426 (2004).

[26] K. Park and M. R. Pederson, Phys. Rev. B **70**, 054414 (2004).

[27] N. Chakov et al., Inorg. Chem. **44**, 5304 (2005).

[28] Model parameters (energies in [meV]) ( $S_{n,0}, S_{n,1}$ ) = (10, 9), ( $D_{n,0}, D_{n,1}$ ) = (0.056, 0.04)  $\Delta_n$  = 4.0 and  $B_2$  =  $10^{-45}$ . Parameters for CCS: ( $S_{n-1,0}, S_{n-1,1}$ ) = ( $9\frac{1}{2}, 9\frac{1}{2}$ ), ( $D_{n-1,0}, D_{n-1,1}$ ) = (0.02, 0.05),  $\Delta_{n-1}$  = 1.3,  $\Gamma_L/\Gamma_R$  = 2, and  $T$  = 2 K. Parameters for NDC: ( $S_{n+1,0}, S_{n+1,1}$ ) = ( $9\frac{1}{2}, 9\frac{1}{2}$ ), ( $D_{n+1,0}, D_{n+1,1}$ ) = (0.02, 0.02),  $\Delta_{n+1}$  = 0.6,  $B_2$  =  $10^{-5}$ ,  $\Gamma_L/\Gamma_R$  = 10, and  $T$  = 1 K. The NDC strength can only be reproduced for a temperature lower than the experimental one in Fig. 2, 3.